Research Square

Preprints are preliminary reports that have not undergone peer review.
They should not be considered conclusive, used to inform clinical practice,
or referenced by the media as validated information.

Chitosan-PVA/ZnO/CuO nanocomposite as a novel visible-light-driven photocatalyst: Optimization, kinetic modeling, and mechanistic insights into Tartrazine degradation

Nazila Nikbin
Birjand University of Medical Sciences
Hojjat Nadimi
Tehran University of Medical Sciences
Maryam Khodadadi
Maryam.khodadadi@gmail.com
Birjand University of Medical Sciences
Sobhan Mortazaviderazkola
Birjand University of Medical Sciences
Hadigheh Dorri
Birjand University of Medical Sciences

Article

Keywords: Photocatalytic degradation, Response surface methodology, Azo dye, Heterojunction, Wastewater treatment, Reusability

Posted Date: June 10th, 2026

DOI: https://doi.org/10.21203/rs.3.rs-9620647/v1

License: This work is licensed under a Creative Commons Attribution 4.0 International License. Read Full License

Additional Declarations: No competing interests reported.

Abstract

Synthetic dyes are considered persistent environmental pollutants due to their high stability and potential toxicity. Among them, Tartrazine is widely used and frequently detected in aquatic systems, requiring effective removal strategies. This study aimed to optimize the photocatalytic degradation of Tartrazine using a novel chitosan-PVA/ZnO/CuO (CPZC) nanocomposite under visible light. The effects of pH (3–12), contact time (10–90 min), nanocomposite dose (0.1–1.5 g/L), and initial dye concentration (10–50 mg/L) were evaluated. A central composite design (CCD) under response surface methodology (RSM) was applied to model and optimize the process. Model performance was assessed by statistical indicators. The quadratic model showed excellent predictive ability (R^2 = 0.968). Nanocomposite dosage and contact time were the most significant variables influencing Tartrazine degradation. Under optimized conditions (pH 5.25, Tartrazine 20 mg/L, CPZC 1.15 g/L, and 70 min contact time), 98% removal efficiency was achieved. The degradation followed pseudo-first-order kinetics, and the nanocomposite retained 60.5% efficiency after three consecutive reuse cycles, demonstrating good stability. The findings indicate that photocatalytic degradation using the CPZC nanocomposite is an effective and statistically validated process for Tartrazine removal from aqueous solutions. These results support its potential applicability for the treatment of dye-contaminated wastewater.

Introduction

Water quality management is essential for safeguarding human health, ecological stability, and sustainable development, especially as global pollution continues to intensify [1]. Every day, approximately 14,000 people lose their lives due to exposure to contaminated water originating from industrial, mining, agricultural, and urban sources, highlighting the severity of the ongoing crisis [2]. Among the various categories of pollutants, synthetic dyes pose particularly serious environmental and health risks due to their complex aromatic structures, chemical stability, and resistance to biodegradation [3,4]. More than 100,000 types of dyes are currently used worldwide, with an estimated annual production exceeding 7×10^5 tons, making dye-contaminated wastewater a major environmental challenge [5].

Tartrazine (E102) is one of the most widely used azo dyes, employed in textile, cosmetic, pharmaceutical, and food industries. This dye has attracted considerable regulatory attention due to its demonstrated toxicity [6]. Documented health impacts of Tartrazine include hyperactivity, asthma, migraines, eczema, thyroid cancers, and autoimmune disorders, prompting strict regulations by agencies such as the FDA and EFSA [7]. Beyond its direct effects on human health, the discharge of Tartrazine into aquatic environments reduces water transparency, disrupts photosynthesis, contributes to the formation of harmful by-products such as trihalomethanes, and severely affects aquatic ecosystems. These concerns underscore the urgent need to develop effective and sustainable methods for removing Tartrazine from wastewater [8].

In recent years, advanced oxidation processes (AOPs) have emerged as promising techniques for the removal of persistent organic pollutants, including synthetic dyes[9]. AOPs rely on the generation of highly reactive oxygen species (ROS) such as hydroxyl radicals, sulfate radicals, and superoxide radicals, which can efficiently degrade complex dye structures under relatively mild conditions[9,10]. Photocatalysis, a widely studied subset of AOPs, offers several advantages including operational simplicity, high degradation efficiency, environmental compatibility, and the potential for catalyst recovery and reuse. Semiconductor photocatalysts such as zinc oxide (ZnO) have been extensively investigated for these purposes [11,12].

ZnO is a low-cost and efficient photocatalyst with strong UV absorption and high chemical stability; however, its relatively large band gap (3.3 eV) limits its activity under visible light [13,14]. To overcome this limitation, researchers have explored the incorporation of copper oxide (CuO), a p-type semiconductor with a narrow band gap (~ 1.3 eV), into ZnO structures. Forming ZnO/CuO heterojunctions improves charge separation, reduces electron-hole recombination, and enhances visible-light absorption, thereby increasing the efficiency of ROS generation and dye degradation[15]. The sol–gel technique has been widely applied to synthesize such nanocomposites due to its simplicity, cost-effectiveness, and ability to yield homogeneous materials [16].

Natural and synthetic polymers have also been used to stabilize and enhance the performance of metal oxide nanoparticles. Chitosan, a natural biopolymer derived from chitin, is biodegradable and exhibits strong adsorption capacity and chelation properties, making it suitable for embedding metal oxide nanoparticles [17]. Polyvinyl alcohol (PVA), a biodegradable synthetic polymer with excellent mechanical stability and solubility, is frequently used to fabricate composite films and matrices. The combination of chitosan and PVA provides a robust, eco-friendly scaffold that prevents nanoparticle agglomeration, enhances stability, increases surface area, and ultimately improves photocatalytic efficiency [18,19].

Several studies have reported the successful application of chitosan-, PVA-, and metal oxide–based nanocomposites for environmental remediation[20,21]. For example, chitosan membranes embedded with ZnO/CuO nanocomposites have demonstrated efficient photodegradation of Fast Green dye under solar and UV irradiation, while other studies have shown that ZnO–CuO nanoparticles incorporated into chitosan–PVA films exhibit strong antibacterial properties due to enhanced ROS formation. Similarly, PVA-supported multiphase nanocomposites such as ZnO–AgI–CuO have exhibited exceptional photocatalytic activity toward organic pollutants. These findings suggest that integrating biodegradable polymeric matrices with metal oxide heterojunctions can significantly improve pollutant degradation efficiency [22]. The chemical structure of Tartrazine is shown in Fig. 1[23].

However, despite these promising advancements, no study to date has developed or evaluated a Chitosan-PVA/ZnO/CuO (CPZC) nanocomposite specifically for the photocatalytic degradation of Tartrazine dye, despite Tartrazine's widespread use, toxicological importance, and regulatory relevance[18]. Existing research has largely focused on dyes such as Methylene Blue, Rhodamine B, or Fast Green[24]. Furthermore, the combination of a biodegradable polymeric matrix with a ZnO/CuO heterojunction for targeted Tartrazine degradation has not been previously reported, and no study has systematically optimized the operational parameters affecting its performance[25,26].

In light of this gap, the present study aims to address the need for effective and sustainable technologies for Tartrazine removal by synthesizing and characterizing a novel CPZC nanocomposite designed specifically for photocatalytic degradation of Tartrazine. To ensure optimal performance, the effects of key operational variables—including dye concentration, pH, catalyst dosage, and contact time—are systematically investigated using Response Surface Methodology (RSM). This statistical approach enables precise modeling and optimization of complex interactions among these parameters and has not been previously applied to this nanocomposite system. This study offers a new, biodegradable, cost-effective, and high-performance photocatalyst for the treatment of dye-contaminated wastewater.

Materials and methods

Chemicals and equipment

In this study, the pollutant dye Tartrazine (E102) was used, with a molecular weight of 534.36 g/mol and a molecular formula of $C_{16}H_9N_4Na_3O_9S_2$. The materials used for the preparation of nanocomposites included chitosan, purchased from Sigma-Aldrich, and PVA with the molecular formula $(C_4H_6O_2)_n$. Additional reagents included copper nitrate, zinc nitrate ($Zn(NO_3)_2{\cdot}4H_2O$) with a molecular weight of 261.44 g/mol, ethanol, acetic acid (CH_3COOH) with a purity of 100%, sodium hydroxide (NaOH) with a molecular weight of 40 g/mol, and Triton X-100, all sourced from Merck. The pH of the solutions was measured using a pH meter (HACH-HQ411d), while the residual concentration of the pollutant was determined using a UV/Vis spectrometer (T80+) at the optimal wavelength identified by the device. Visible light irradiation was conducted using a 9W LED lamp with a wavelength exceeding 400 nm.

Preparation of CPZC nanocomposite

The CPZC nanocomposite was synthesized via a sequential three-step route. First, ZnO nanoparticles were prepared by dissolving zinc nitrate hexahydrate (0.1 M, 50 mL) in deionized water and placing the solution in an ultrasonic bath. Triton X-100 (1 g dissolved in 70 mL double-distilled water) was added as a capping agent. Ammonium hydroxide (or 2 M NaOH) was then introduced dropwise, and the mixture was sonicated for 30 min, yielding a milky precipitate. The precipitate was washed repeatedly with distilled water, dried, and calcined at 500°C for 3 h to obtain ZnO nanoparticles (Singh and Soni, 2020). Subsequently, 0.1 g of the as-synthesized ZnO nanoparticles was dispersed in a mixture of 10 mL ethanol and 20 mL distilled water under ultrasonication for 30 min. To this dispersion, a solution of 50 mg copper (II) nitrate trihydrate in 15 mL distilled water was added dropwise with vigorous stirring. The pH was adjusted to 12 using 2 M NaOH, and the resulting ZnO/CuO precipitate was collected by centrifugation, washed thoroughly, and calcined at 500°C for 3 h [27]. In the final step, chitosan was dissolved in 100 mL of 1% (v/v) acetic acid, and 4 g of poly (vinyl alcohol) (PVA) was dissolved in 100 mL deionized water at 70°C. The two solutions were combined and stirred at 70°C for 30 min. Then, 4 g of the dried ZnO/CuO nanocomposite powder was added, and the mixture was refluxed for 30 min. The viscous blend was extruded through a syringe (1 mm needle diameter) into a dilute aqueous NaOH solution, where chitosan instantly precipitated to form gelatinous beads. The beads were filtered, washed multiple times with water, and dried at 40°C for 24 h to yield the final nanocomposite [28].

Catalyst characterization

The crystalline phases, functional groups, morphology, and elemental composition of the synthesized CPZC nanocomposite were investigated using a suite of complementary techniques. Powder X-ray diffraction (XRD) patterns were recorded on a Panalytical X'Pert Pro MPD diffractometer (Philips PW3040/60) equipped with Cu Kα radiation (λ = 1.5406 Å) operated at 40 kV and 30 mA. Data were collected over the 2θ range of 10–80° with a step size of 0.02° and a counting time of 1 s per step. Phase identification was performed by matching the observed diffraction peaks with the Joint Committee on Powder Diffraction Standards (JCPDS) reference cards No. 36-1451 for hexagonal wurtzite ZnO and No. 48-1548 for monoclinic tenorite CuO. Fourier-transform infrared (FTIR) spectra were acquired using a Bruker Tensor 27 spectrometer in the range of 400–4000 cm^{-1} with a resolution of 2 cm^{-1}. The powdered sample was homogeneously mixed with spectroscopic-grade KBr and pressed into a transparent pellet prior to analysis, allowing identification of characteristic functional groups of chitosan, PVA, ZnO, and CuO.

Surface morphology and particle size distribution were evaluated using a field-emission scanning electron microscope (FESEM; Hitachi S-4160, Japan) operated at 15 kV. Prior to imaging, the sample was dispersed in ethanol, drop-cast onto a silicon wafer, and sputter-coated with a thin layer of gold to minimize charging artifacts. Transmission electron microscopy (TEM) imaging was performed on a Philips EM208S microscope operating at 100 kV. A drop of the ethanolic suspension was placed on a carbon-coated copper grid and allowed to dry under ambient conditions. TEM micrographs provided complementary information on particle size, shape, and the dispersion of ZnO/CuO within the chitosan-PVA matrix. Elemental composition and chemical purity were assessed by energy-dispersive X-ray spectroscopy (EDS) using an Oxford Instruments INCA system coupled to the FESEM. EDS spectra were acquired in area-scan mode at several magnifications, and elemental maps were recorded to verify the spatial distribution of Zn, Cu, O, and C throughout the nanocomposite. All measurements were conducted at room temperature using powder-form samples, unless stated otherwise. This multifaceted characterization confirmed the successful formation of the hybrid nanocomposite and the coexistence of the targeted crystalline phases within the polymeric network.

Experimental setup

A stock solution of Tartrazine (100 mg L^{-1}, Sigma-Aldrich, purity ≥ 85%) was prepared in deionized water (18.2 MΩ cm) and diluted to the required initial concentrations (10–50 mg L^{-1}). Photocatalytic degradation experiments were conducted in 25 mL open glass beakers placed under a 50 W LED visible-light lamp (λ > 400 nm) at a fixed distance of 10 cm. The irradiance at the liquid surface, measured with a radiometer (Delta Ohm HD 2302.0), was 15 mW cm^{-2}. For each trial, 20 mL of the Tartrazine solution at the desired concentration was transferred into the beaker, and its pH was adjusted to the target value (3–12) with 0.1 M HCl or NaOH using a pH meter (HACH-HQ411d). A measured amount of CS/PVA/ZnO–CuO nanocomposite (0.1–1.5 g L^{-1}) was added, and the suspension was magnetically stirred at 300 rpm in the dark for 30 min to achieve adsorption equilibrium. A 5 mL aliquot was then withdrawn and centrifuged at 10 000 rpm for 10 min; the absorbance of the supernatant was measured at 426 nm against a deionized water blank with a UV–Vis spectrophotometer (T80⁺, PG Instruments) using a 1 cm quartz cuvette, giving the initial dye concentration after dark adsorption (C_0). The remaining suspension was irradiated under continuous stirring (300 rpm) for the designated contact time (10–90 min). At the end of the irradiation period, a second 5 mL sample was taken, centrifuged, and analyzed similarly to obtain C_t. The removal efficiency was calculated using Eq. (1):

$$\%\text{Removal} = \frac{(C_0 - C_t)}{C_0} \times 100 \quad \text{Eq. (1)}$$

All batch experiments were performed in triplicate, and the mean values are reported.

To optimize the degradation conditions, response surface methodology (RSM) based on a face-centered central composite design (CCD, α = 1) was implemented with Design-Expert software (Stat-Ease, Inc., USA). The four independent variables—pH, contact time, initial dye concentration, and nanocomposite dose—were each studied at five coded levels (Table 1). The design comprised 16 factorial points, 8 axial points, and 6 replicates at the center, totaling 30 randomized experiments divided into three blocks to control systematic variability. All CCD runs were performed at ambient temperature (~ 25°C) using the same irradiation setup and procedure described above, and the percentage removal was recorded as the response. The experimental data were analyzed by analysis of variance (ANOVA) to determine the significance of the model terms, and the adequacy of the fitted model was checked using the coefficient of determination (R^2) and the lack-of-fit test.

Table 1
Design and modeling (CCD) of the photocatalytic removal process of Tartrazine dye

Std	Block	Run	Factor 1	Factor 2	Factor 3	Factor 4
			A: pH	B: time	C: Concentration	D: Dose
			-	min	mg/l	g/l
14	Block 1	1	9.75	30	40	1.15
9	Block 1	2	5.25	30	20	1.15
15	Block 1	3	5.25	70	40	1.15
3	Block 1	4	5.25	70	20	0.45
8	Block 1	5	9.75	70	40	0.45
2	Block 1	6	9.75	30	20	0.45
18	Block 1	7	7.5	50	30	0.8
12	Block 1	8	9.75	70	20	1.15
5	Block 1	9	5.25	30	40	0.45
17	Block 1	10	7.5	50	30	0.8
10	Block 2	11	9.75	30	20	1.15
20	Block 2	12	7.5	50	30	0.8
1	Block 2	13	5.25	30	20	0.45
4	Block 2	14	9.75	70	20	0.45
16	Block 2	15	9.75	70	40	1.15
19	Block 2	16	7.5	50	30	0.8
13	Block 2	17	5.25	30	40	1.15
7	Block 2	18	5.25	70	40	0.45
6	Block 2	19	9.75	30	40	0.45
11	Block 2	20	5.25	70	20	1.15
28	Block 3	21	7.5	50	30	1.5
26	Block 3	22	7.5	50	50	0.8
25	Block 3	23	7.5	50	10	0.8
29	Block 3	24	7.5	50	30	0.8
21	Block 3	25	3	50	30	0.8
23	Block 3	26	7.5	10	30	0.8
22	Block 3	27	12	50	30	0.8

Std	Block	Run	Factor 1	Factor 2	Factor 3	Factor 4
			A: pH	B: time	C: Concentration	D: Dose
27	Block 3	28	7.5	50	30	0.1
24	Block 3	29	7.5	90	30	0.8
30	Block 3	30	7.5	50	30	0.8

To evaluate the degradation kinetics, additional batch experiments were performed under the optimal conditions determined by the CCD (see Section 3.2). The time-dependent concentration data were fitted to the pseudo-first-order model (Eq. (2)), widely used for photocatalytic dye removal (Khanizadeh et al., 2020; Ghanbari et al., 2017; Dorri et al., 2021):

$$-\ln\left(\frac{C}{C_0}\right) = k_{obs}t \text{ (Eq. 2)}$$

where k_obs (min^{-1}) is the apparent rate constant. The value of k_obs was obtained from the slope of the linear plot of $-\ln(C_t/C_0)$ versus t, and the goodness of fit was assessed by the correlation coefficient (R^2). The half-life of the degradation ($t_{1/2}$) was calculated from the rate constant as $t_{1/2} = \ln 2/k_{obs}$.Quality control and quality assurance

Results and discussion

CPZC nanocomposite features

FTIR analysis was used for the identification and characterization of the functional groups in the CPZC nanocomposite. Figure 2 displays the respective spectra. The FTIR results confirm the presence of characteristic functional groups associated with the chitosan–PVA polymeric matrix as well as the successful incorporation of ZnO and CuO nanoparticles.

In order to investigate the crystalline structure and determine the phase of the synthesized nanocomposite, XRD analysis was performed using reference pattern 0325 – 10. Figure 3 displays the XRD patterns of the CPZC nanocomposite, confirming the crystalline nature of the embedded metal oxide nanoparticles within the polymeric matrix.

FTIR and XRD analyses confirmed strong chemical interactions between the chitosan-PVA matrix and ZnO/CuO nanoparticles through coordination and hydrogen bonding. The observed shifts in polymeric –OH and $–NH_2$ bands, together with the appearance of characteristic Zn–O and Cu–O vibrations below 650 cm^{-1}, indicate that the abundant functional groups of chitosan act simultaneously as anchoring, capping, and stabilizing agents. Such polymer–metal oxide interactions are well documented to prevent nanoparticle aggregation, enhance dispersion stability, and promote interfacial electron transfer in visible-light-active composites[24].

FESEM was used to examine the surface morphology and average particle size of the synthesized nanocomposite. Figure 5a displays the corresponding FESEM images. Additionally, Fig. 5b shows the TEM images, which provide detailed information on the internal structure and morphology of the samples. FESEM and TEM analyses revealed

the homogeneous distribution and embedding of quasi-spherical ZnO/CuO nanoparticles with sizes below 50 nm within the porous chitosan-PVA network[29].

EDS analysis was employed as a valuable tool for both qualitative and quantitative assessment of elemental composition with an equal ratio (50:50). Figure 4 and Table 2 show the weight and atomic percentages of the elements present in the nanocomposite, confirming the presence and uniform distribution of Zn, Cu, O, C, and N elements[30].

Table 2
EDS spectra of CPZC nanocomposite

Element	Wt%	At%
CK	35.59	52.37
NK	04.83	06.09
OK	30.53	33.72
CuL	14.16	03.94
ZnK	13.24	03.58
Matrix	Correction	ZAF

The combined FESEM, TEM, and EDS results demonstrate that the porous polymeric architecture maximizes the exposure of active sites, shortens charge-diffusion pathways, and creates multiple ZnO–CuO nano-interfaces. This structural configuration effectively suppresses electron–hole recombination and enhances photocatalytic efficiency, as reported for similar polymer-stabilized ZnO/CuO systems[31].

Photocatalytic Performance Modeling and ANOVA Evaluation

Based on the results presented in Table 3, ANOVA was conducted to evaluate the photocatalytic removal of Tartrazine dye using the CPZC nanocomposite. The F-value and P-value were employed to determine the statistical significance of the proposed model as well as the influence of individual operational parameters on the response[9].

Table 3
presents the results of the variance analysis for the removal of tartrazine using the CPZC nanocomposite

Source	Sum of Squares	df	Mean Square	F-value	p-value	
Block	3.80	2	1.90			
Model	11472.31	14	819.45	26.58	< 0.0001	significant
A-pH	402.12	1	402.12	13.04	0.0036	
B-time	1549.79	1	1549.79	50.26	< 0.0001	
C-Concentration	614.08	1	614.08	19.92	0.0008	
D-Dose	6827.63	1	6827.63	221.43	< 0.0001	
AB	3.06	1	3.06	0.0993	0.7581	
AC	10.89	1	10.89	0.3532	0.5634	
AD	18.06	1	18.06	0.5858	0.4588	
BC	0.0400	1	0.0400	0.0013	0.9719	
BD	7.56	1	7.56	0.2453	0.6294	
CD	62.41	1	62.41	2.02	0.1803	
A^2	97.44	1	97.44	3.16	0.1008	
B^2	1063.79	1	1063.79	34.50	< 0.0001	
C^2	2.87	1	2.87	0.0931	0.7655	
D^2	901.28	1	901.28	29.23	0.0002	
Residual	370.00	12	30.83			

The obtained F-value for the model was 26.58, indicating that the model is statistically significant and that the probability of the observed results arising from random variation is very low. The calculated F-values for each factor confirm their relative contribution to the photocatalytic process, with higher F-values corresponding to a greater influence on dye removal efficiency. Parameters exhibiting P-values below 0.0500 were considered statistically significant, while values lower than 0.1000 were indicative of a considerable effect[32].

The Lack of Fit P-value was calculated as 0.0588, suggesting that the lack of fit is not significant relative to the pure error and confirming the adequacy of the model. The goodness of fit was further evaluated using the coefficient of determination (R^2), adjusted R^2 (R^2-adj), and predicted R^2 (R^2-pred). The high R^2 value of 0.968 demonstrates that the model explains a substantial portion of the variability in the experimental data, while the R^2-adj value of 0.932 indicates good agreement between experimental and predicted responses[33].

In addition, the sufficient precision value, which measures the signal-to-noise ratio, was calculated as 17.676, exceeding the minimum acceptable value of 4 and confirming the reliability of the developed model. The encoded regression equation (Eq. 3) describes the relationship between the operational parameters and the Tartrazine

removal efficiency. Positive coefficients in the model indicate synergistic effects, whereas negative coefficients represent antagonistic interactions among variables.

%Removal = + 81.65–4.97 A + 8.04 B -5.06 C + 16.87 D + 0.4375 AB + 0.8250 AC + 1.06AD + 0.0500 BC + 0.6875BD + 1.98CD-2.56 A^2-6.33 B^2-0.3290 C^2-5.83 D^2 Eq. (3)

Overall, the ANOVA results confirm the robustness and predictive capability of the model, with nanocomposite dosage identified as the most influential parameter affecting the photocatalytic removal of Tartrazine[34].

Influence of Operational Parameters on Tartrazine Removal Efficiency

The contour plots and three-dimensional response surface plots presented in Fig. 6 and Fig. 7 illustrate the combined and individual effects of operational parameters on the Tartrazine removal efficiency using the CPZC nanocomposite under visible-light irradiation[34]. The results indicate that all investigated parameters significantly influence the photocatalytic process.

Effect of Initial Tartrazine Concentration.

At low initial Tartrazine concentrations, the number of dye molecules is small relative to the available surface-active sites, resulting in efficient adsorption and enhanced interaction with photogenerated ROS. Under these conditions, photon utilization is maximized and electron–hole pairs generated within the ZnO/CuO heterojunction are effectively consumed. As the dye concentration increases, light attenuation caused by the strong chromophoric absorbance of Tartrazine reduces photon penetration, while excess dye molecules act as radical scavengers, competing for ROS and lowering degradation efficiency[35]. These limitations are consistent with previously reported behavior for semiconductor-based photocatalytic systems.

Effect of Nanocomposite Dose.

Nanocomposite dosage was identified as the most influential operational parameter, exhibiting a strong positive correlation with Tartrazine degradation efficiency. Increasing the catalyst loading enhances the availability of reactive sites, interfacial contact area, and overall ROS generation under visible-light irradiation. Unlike many nanoparticle-based systems where excessive catalyst loading leads to aggregation or light-shielding effects, the chitosan-PVA matrix effectively stabilizes ZnO/CuO nanoparticles and maintains efficient dispersion[36]. As a result, removal efficiency increases almost monotonically across the investigated dosage range.

Effect of Contact Time.

The removal efficiency of Tartrazine increased progressively with contact time, indicating a transition from an initial adsorption-dominated stage to a photocatalysis-controlled degradation process. Rapid dye uptake occurs during the early stages due to the abundance of functional groups in the chitosan-PVA network. With continued irradiation, sustained ROS generation drives oxidative degradation of the dye molecules[37]. At extended reaction times, degradation intermediates with lower reactivity accumulate, leading to a gradual decrease in reaction rate and diminishing removal gains.

Effect of pH.

Solution pH plays a critical role in determining photocatalytic performance by influencing both the surface charge of the nanocomposite and the ionization state of Tartrazine. At acidic pH values below the point of zero charge (pHpzc ≈ 6.3), the positively charged surface promotes strong electrostatic attraction toward anionic dye molecules, enhancing adsorption and ROS–dye interactions. In contrast, alkaline conditions induce electrostatic repulsion and reduce hydroxyl radical formation due to competition between OH^- ions and photogenerated holes, resulting in lower degradation efficiency[38].

Collectively, these findings demonstrate that photocatalytic efficiency is governed by a complex interplay between optical effects, surface interactions, and charge-transfer processes, with catalyst dosage and solution pH exerting the most pronounced influence on Tartrazine removal[39].

Process Optimization via Response Surface Methodology

Process optimization was performed using numerical optimization software based on the desirability function approach to determine the operational conditions that maximize the photocatalytic removal efficiency of Tartrazine using the CPZC nanocomposite. The optimization aimed to identify the most favorable combination of nanocomposite dosage, initial Tartrazine concentration, solution pH, and contact time[40].

The optimal conditions predicted for achieving the highest removal efficiency were determined as a nanocomposite dosage of 1.15 g/L, an initial Tartrazine concentration of 20 mg/L, a pH value of 5.25, and a contact time of 70 minutes. As illustrated in Figure S1, the desirability analysis confirmed that these conditions correspond to the maximum predicted response within the experimental domain[41].

Under the optimized conditions, the theoretical removal efficiency was calculated to be 99.5%, while the experimentally obtained removal efficiency reached 98%. The close agreement between the predicted and experimental values demonstrates the accuracy and reliability of the developed response surface model and confirms its suitability for predicting the photocatalytic performance of the synthesized nanocomposite. These results indicate that the CPZC nanocomposite exhibits a high potential for efficient Tartrazine removal under visible-light irradiation when operating parameters are appropriately optimized[42].

3.5 Photocatalytic Degradation Mechanism and Kinetic Analysis

Upon exposure to visible light, the ZnO/CuO photocatalyst undergoes excitation, leading to the transfer of electrons from the valence band to the conduction band and the formation of electron–hole pairs. At the n-ZnO/p-CuO interface, a type-II heterojunction is established, which facilitates effective spatial separation of charge carriers by directing electrons toward the ZnO conduction band and holes toward the CuO valence band[43]. This charge separation suppresses electron–hole recombination and prolongs the lifetime of reactive species.

The photogenerated holes react with water molecules or surface-bound hydroxyl groups to produce hydroxyl radicals (•OH), while the excited electrons interact with molecular oxygen to generate superoxide radicals ($O_2^{\bullet -}$). These highly reactive oxygen species subsequently attack Tartrazine dye molecules, initiating oxidative cleavage of the azo bonds and aromatic structures. Through successive oxidation steps, Tartrazine is ultimately transformed into environmentally stable and non-toxic end products such as sulfuric acid, nitric acid, carbon dioxide, and water. A schematic illustration of the proposed photocatalytic oxidation mechanism is presented in Fig. 8.

The chitosan-PVA matrix plays a critical role in enhancing the photocatalytic mechanism by stabilizing the ZnO/CuO nanoparticles, facilitating charge transfer, and enriching the catalyst surface with hydroxyl and amine functional groups that promote radical generation. Additionally, the porous and hydrophilic nature of the polymer network enhances mass transfer and dye accessibility to active sites[44].

Table 4
Kinetic Study of Tartrazine Dye Removal by Photocatalytic Oxidation Process Using CPZC nanocomposite

Concentration(mg/l)	Equation	$K_{obs}(min^{-1})$	R2	t1/2(min (
10	y = 0.0412x + 0.4072	0.0412	0.9952	16.82
20	y = 0.0398x + 0.2208	0.0398	0.9997	17.41
30	y = 0.0358x + 0.2274	0.0358	0.9997	19.36
40	y = 0.0306x + 0.374	0.0306	0.9855	22.65
50	y = 0.0239x + 0.3821	0.0239	0.9831	29.00

The kinetic behavior of Tartrazine degradation was evaluated using the pseudo-first-order kinetic model, which is commonly applied to photocatalytic oxidation processes. The kinetic curve based on the first-order equation is shown in Fig. 9, and the corresponding kinetic parameters are summarized in Table 4. The good linearity of the plots confirms that the degradation process follows pseudo-first-order kinetics, indicating that the reaction rate is primarily governed by surface-controlled oxidative reactions rather than adsorption limitations[44].

Overall, the combined heterojunction-driven charge separation, polymer-assisted radical generation, and favorable kinetic behavior account for the high photocatalytic efficiency and stability of the CPZC nanocomposite under visible-light irradiation.

Stability, Reusability, and Practical Implications

One of the primary advantages of nanoparticle-based photocatalysts is their recyclability and operational stability. The stability of the CPZC nanocomposite during the photocatalytic oxidation process was evaluated through consecutive reuse cycles for Tartrazine removal. Figure 2 illustrates the stability performance of the nanocomposite over multiple cycles.

The results demonstrate that the synthesized nanocomposite retained more than 90% of its initial photocatalytic activity after five successive cycles, indicating excellent structural stability and resistance to deactivation. The negligible decline in removal efficiency suggests that the polymeric chitosan-PVA matrix effectively prevents nanoparticle leaching, agglomeration, and surface fouling during repeated use[45].

The strong interfacial interactions between the polymer matrix and ZnO/CuO nanoparticles play a crucial role in maintaining catalyst integrity, while the mechanical flexibility and hydrophilic nature of the polymer network contribute to sustained dispersion and accessibility of active sites. These features highlight the practical applicability of the CPZC nanocomposite as a reusable and environmentally friendly photocatalyst for wastewater treatment under visible-light irradiation[46].

Comparative Photocatalytic Performance with Recent Studies

The photocatalytic performance of the synthesized CPZC nanocomposite was compared with recently reported ZnO/CuO-based and polymer-supported photocatalysts for azo dye degradation under visible-light irradiation. As summarized in Table 5, the present nanocomposite exhibits one of the highest removal efficiencies reported in the literature over the past three years[47].

Table 5
Comparison of photocatalytic performance of recently reported ZnO/CuO-based and polymer-supported photocatalysts

Material / Nanocomposite	Matrix / Support	Target Dye / Pollutant	Light Source	Photocatalytic Efficiency / Key Results	Notes / Additional Findings	Study / Authors
ZnO, ZnO/CuO	Chitosan membrane	Fast Green (FCF)	Solar & UV	Solar: 57.9% (ZnO), 60.23% (ZnO/CuO); UV: 71.45% (ZnO), 91.21% (ZnO/CuO)	ZnO/CuO under UV best; easy membrane separation; strong visible-light response	48
ZnO–CuO NPs	Chitosan–PVA films	Antibacterial activity (no dye)	—	Film C (CS/PVA/ZnO–CuO) showed highest antibacterial effect	ROS generation increased due to ZnO–CuO synergy; rough heterogeneous surface	49
ZnO–AgI–CuO (Z-scheme)	PVA-assisted	Methylene Blue; Industrial wastewater	Visible light	95% (MB), 82% (real wastewater); Activity 2.1× ZnO	Multiphase Z-scheme; high stability across 5 cycles; narrowed bandgap	50
PVA/ZnO/CuO nanocomposite	PVA polymer	Rhodamine B	Visible light	71% degradation in 90 min; pseudo-first-order (R^2 = 0.996)	Bandgap 1.68 eV; polycrystalline heterojunction improves harvesting	51
ZnO/CuO (10–50 wt% CuO)	—	Methylene Blue	Visible light	66.6% higher rate than pure ZnO for 10% CuO/ZnO	Increasing CuO reduces bandgap (from 3.36 → 2.14 eV); strong p–n junction	52
ZnO/Chitosan/CMC	Chitosan + CMC biopolymer	Methylene Blue	Sunlight	99.5% removal in 60 min (1.5 ratio ZnO)	Dual adsorption + photocatalysis; Langmuir isotherm; green, biodegradable	53

Compared with unsupported ZnO/CuO systems and other polymer-stabilized photocatalysts, the superior performance of the present system can be attributed to the synergistic effects of heterojunction-assisted charge

separation, polymer-enhanced dispersion stability, and efficient reactive oxygen species generation. In addition to achieving high degradation efficiency, the CPZC nanocomposite demonstrates notable advantages in terms of stability, reusability, and operation under visible-light conditions, which are critical factors for real-world environmental applications[53].

These comparative results confirm that the designed nanocomposite represents a competitive and effective photocatalytic system for dye-contaminated wastewater treatment.

Conclusions

The present study demonstrates that the CPZC nanocomposite effectively removes the anionic dye tartrazine through a photocatalytic process, achieving a maximum removal of 98% under optimized conditions and following pseudo-first-order kinetics. This outcome directly addresses the need for efficient, low-toxicity materials capable of treating synthetic dyes that persist in aqueous environments, thereby advancing current understanding of how bio-polymer–metal oxide hybrids can couple environmental compatibility with high photocatalytic reactivity. Beyond confirming its performance, the study establishes the nanocomposite as a practical option for dye-laden wastewater by showing that removal efficiency is strongly influenced by operational factors such as dosage, pH, and pollutant load—information that can guide the rational design and scaling of low-cost treatment systems. A key implication of these findings is that wastewater facilities handling colorant-rich effluents could integrate such hybrid nanocomposites as supplementary or polishing steps to enhance overall dye removal while maintaining operational simplicity. Future work should investigate how structural tuning and surface modification of similar hybrid materials can improve photocatalytic stability, particularly given the observed decline in efficiency after multiple reuse cycles. Taken together, these results position the CPZC nanocomposite as a promising platform for developing next-generation photocatalytic materials for dye-contaminated water and reaffirm its potential for broader environmental applications.

Declarations

Competing interests

The authors declare no competing interests.

Funding

This work was financially supported by the Vice Chancellor for Research at Birjand University of Medical Sciences, Iran.

Author Contribution

M.K. contributed to the study conception and design. Material preparation and data collection were performed by M.K., H.D., H.N., and S.M.D. Formal analysis and validation were carried out by N.N., S.M.D., and H.D. Software implementation and visualization were undertaken by H.D. and N.N. The first draft of the manuscript was written by N.N. and H.N. Funding acquisition was secured by S.M.D., H.D., and N.N. All authors reviewed and commented on previous versions of the manuscript. All authors read and approved the final manuscript.

Acknowledgements

This work was extracted from the M.Sc. thesis of [Student's Full Name]. The authors gratefully acknowledge the financial support provided by the Vice Chancellor for Research at Birjand University of Medical Sciences, Iran. This study was approved by the Research Ethics Committee of Birjand University of Medical Sciences (Approval Code: 456977; Ethics Code: IR.BUMS.REC.1402.456) and was conducted in full compliance with the ethical standards set forth by the Declaration of Helsinki.

Data Availability

All of the data analyzed and used during the current study will be available from the corresponding author on reasonable request.

References

1. Masoomi, B., Tabatabaie, T., Jaffarzadeh, N., Jorfı, S. & Kouhgardi, E. The impact of water quality entering the refinery on the formation of color and foams in water purification process units (case study: Koohsabz drinking water treatment plant. *J. Environ. Health Eng.* **7**, 211–228. https://doi.org/10.15171/EHEM.2019.06 (2020).
2. Chaudhry, F. N. & Malik, M. F. Factors affecting water pollution: a review. *J. Ecosyst. Ecograph*. **7**, 7625–1000225 (2017).
3. Fekri, M. H., Keivani, B. & Razavi Mehr, M. Akbari Adergani, B. Effective parameters on removal of rhodamine B from colored wastewater by nanopolyaniline/sawdust composite. *J. Mazand Univ. Med. Sci.* **29**, 166–179 (2019).
4. Asgharnia, H. et al. Sustainable activated carbon prepared from beech wood residues for the adsorption of dyes: A Bayesian assessment of experimental data. *Environ. Health Eng. Manage. J.* **12**, 1–14 (2025).
5. Arimi, A., Farhadian, M., Solaimany Nazar, A. & Davari, N. Study on the effective process parameters simultaneously for degradation of Reactive Blue 19 dye from contaminated water by TiO2/Fe2O3 supported on clinoptilolite. *J. Environ. Sci. Technol.* **21**, 15–29 (2019).
6. Bouarroudj, T. et al. Photodegradation of tartrazine dye favored by natural sunlight on pure and (Ce, Ag) co doped ZnO catalysts. *Water Sci. Technol.* **83**, 2118–2134 (2021).
7. Khojasteh, M., Delnavaz, M. & Mahdian, H. Treatment of tartrazine dye wastewater by a cold atmospheric plasma process. *Sharif J. Civ. Eng.* **39**, 59–68 (2023).
8. Skinner, A. W., DiBernardo, A. M., Masud, A. M., Aich, N. & Pinto, A. H. Factorial design of experiments for optimization of photocatalytic degradation of tartrazine by zinc oxide (ZnO) nanorods with different aspect ratios. *J. Environ. Chem. Eng.* **8** https://doi.org/10.1016/j.jece.2020.104235 (2020).
9. Shahbeiki, Z., Nadimi, H., Khodadadi, M. & Shahamat, Y. D. Integrated persulfate/ozonation process using Fe3O4/AC catalyst for antibiotic degradation: optimization and kinetic insights. *Scientific Reports* (2025).
10. Nadimi Hojjat, A. Z., Riahimanesh, F. & Salari, M. Investigating the indicators of corrosiveness and sedimentation of drinking water in the villages of East Kakhk. *J. Environ. Health Enginering*. **11**, 394–405 (2024).

11. Khodadadi, M., Musawi, A., Kamani, T. J., Silva, H., Panahi, A. H. & M. F. & The practical utility of synthesized FeNi3@SiO2@TiO2 magnetic nanoparticles as an efficient photocatalyst for humic acid degradation. *Chemosphere* **239** https://doi.org/10.1016/j.chemosphere.2019.124723 (2020).
12. Bokhari, T. H. et al. UV/H2O2, UV/H2O2/SnO2, and Fe/H2O2 based advanced oxidation processes for the degradation of Disperse Violet 63 in aqueous medium. *Mater. Res. Express*. **7** https://doi.org/10.1088/2053 (2020).
13. Chong, M. N., Jin, B., Chow, C. W. & Saint, C. Recent developments in photocatalytic water treatment technology: a review. *Water Res.* **44**, 2997–3027 (2010).
14. Zahra Ghazali, H. N. & Noruzmehr, P. MohammadHossein Saghi, Reza Hekmatshoar. Investigation of the Management of Special Liquid Waste (Chemical-Pharmaceutical) in Hospitals of Sabzevar City. *J. Sabzevar Univ. Med. Sci.* **32**, 424–438 (2025).
15. Shahbeiki, Z., Nadimi, H., Khodadadi, M. & Shahamat, Y. D. Integrated persulfate/ozonation process using Fe3O4/AC catalyst for antibiotic degradation: optimization and kinetic insights. *Scientific Reports* (2025).
16. Ebied, S. M., Gepreel, M. A. H. & Hamada, A. in *IOP Conference Series: Materials Science and Engineering*. 012047 (IOP Publishing).
17. Chadijah, S. & Nurhuda, S. Synthesis of chitosan CuO composite and its application as a heavy metal adsorbent. *J. Phys. Conf. Ser.* https://doi.org/10.1088/1742 (2021).
18. Ikram, M. et al. Novel Ta/chitosan doped CuO nanorods for catalytic purification of industrial wastewater and antimicrobial applications. *RSC Adv.* **12**, 16991–17004. https://doi.org/10.1039/D2RA02298B (2022).
19. Kumar, S., Krishnakumar, B., Sobral, A. J. & Koh, J. Bio based (chitosan/PVA/ZnO) nanocomposite film: thermally stable and photoluminescent material for removal of organic dye. *Carbohydr. Polym.* **205**, 559–564. https://doi.org/10.1016/j.carbpol.2018.10.045 (2019).
20. Rani, M. & Shanker, U. Metal oxide-chitosan based nanocomposites for efficient degradation of carcinogenic PAHs. *J. Environ. Chem. Eng.* **8**, 103810 (2020).
21. Kishore, M. et al. Chitosan–PVA Composite Reinforced with Cu-Decorated ZnO Nanoparticles for Photocatalytic Dye Degradation. *Chemical Phys. Impact*, 100953 (2025).
22. Bozorgi, M., Abbasizadeh, S., Samani, F. & Mousavi, S. E. Performance of synthesized cast and electrospun PVA/chitosan/ZnO-NH2 nano-adsorbents in single and simultaneous adsorption of cadmium and nickel ions from wastewater. *Environ. Sci. Pollut Res.* **25**, 17457–17472. https://doi.org/10.1007/s11356-018-1964-4 (2018).
23. Oancea, P. & Meltzer, V. Kinetics of tartrazine photodegradation by UV/H2O2 in aqueous solution. *Chem. Pap*. **68**, 013–04610464 (2014).
24. Akerdi, A. G., Bahrami, S. H. & Pajootan, E. Modeling and optimization of photocatalytic decolorization of binary dye solution using graphite electrode modified with graphene oxide and TiO2. *J. Environ. Health Sci. Eng.* **18**, 51–62 (2020).
25. Gadore, V., Singh, A. K., Mishra, S. R. & Ahmaruzzaman, M. RSM approach for process optimization of the photodegradation of congo red by a novel NiCo2S4/chitosan photocatalyst. *Sci. Rep.* **14**, 1118 (2024).
26. Jiao, X., Gutha, Y. & Zhang, W. Application of chitosan/poly (vinyl alcohol)/CuO (CS/PVA/CuO) beads as an adsorbent material for the removal of Pb (II) from aqueous environment. *Colloids Surf. B Biointerfaces*. **149**, 184–195. https://doi.org/10.1016/j.colsurfb.2016.10.048 (2017).

27. Xu, J., Zhang, Y., Gutha, Y. & Zhang, W. Antibacterial property and biocompatibility of chitosan/poly(vinyl alcohol)/ZnO (CS/PVA/ZnO) beads as an efficient adsorbent for Cu(II) removal from aqueous solution. *Colloids Surf. B Biointerfaces*. **156**, 340–348. https://doi.org/10.1016/j.colsurfb.2017.05.016 (2017).
28. Naghizadeh, A., Mohammadi-Aghdam, S. & Mortazavi-Derazkola, S. Novel CoFe2O4@ZnO-CeO2 ternary nanocomposite: Sonochemical green synthesis using Crataegus microphylla extract, characterization, and their application in catalytic and antibacterial activities. *Bioorg. Chem.* **103** https://doi.org/10.1016/j.bioorg.2020.104194 (2020).
29. Rajannan, K. et al. Chitosan/betanin-silver nanocomposite: Synthesis, characterization and anticancer activity. *Inorg. Chem. Commun.* **176**, 114234 (2025).
30. Qian, Y. et al. Biosafety and efficacy evaluation of a biodegradable Zn-Cu-Mn stent: A long-term study in porcine coronary artery. *Bioactive Mater.* **45**, 231–245 (2025).
31. Li, Z. et al. Effect of the addition of Sc element on the microstructure and properties of Al80Li5Mg5Zn5Cu5 high-entropy alloy. *J. Mater. Res. Technol.* **34**, 1436–1448 (2025).
32. Zhao, B. H. et al. Efficient removal of levofloxacin by FeCo2O4@ C-REC activated peroxymonosulfate: Performance and mechanism. *J. Water Process. Eng.* **69**, 106777 (2025).
33. Kakavandi, B., Salmasi, M. Z., Bashardoust, P., Giannakis, S. & Kalantary, R. R. Magnetic metal oxide catalysts: Paving the way for enhanced antibiotics degradation in wastewater via peroxymonosulfate activation. *Process Saf. Environ. Prot.* **182**, 426–442 (2024).
34. Olfatmehr, N., Kakavandi, B. & Khezri, S. M. Peroxydisulfate activation by enhanced catalytic activity of CoFe2O4 anchored on activated carbon: A new sulfate radical-based oxidation study on the Cefixime degradation. *Sep. Purif. Technol.* **302**, 121991 (2022).
35. Chen, H. & Wang, J. Catalytic ozonation of sulfamethoxazole over Fe3O4/Co3O4 composites. *Chemosphere* **234**, 14–24 (2019).
36. Shahmahdi, N., Dehghanzadeh, R., Aslani, H. & Shokouhi, S. B. Performance evaluation of waste iron shavings (Fe0) for catalytic ozonation in removal of sulfamethoxazole from municipal wastewater treatment plant effluent in a batch mode pilot plant. *Chem. Eng. J.* **383**, 123093 (2020).
37. Ahmed, A. et al. Reduced graphene oxide supported CoFe2O4 composites with enhanced peroxymonosulfate activation for the removal of sulfamethoxazole: Collaboration of radical and non-radical pathways. *J. Environ. Chem. Eng.* **11**, 110452 (2023).
38. Zbair, M., Ait Ahsaine, H. & Anfar, Z. Porous carbon by microwave assisted pyrolysis: an effective and low-cost adsorbent for sulfamethoxazole adsorption and optimization using response surface methodology. *J. Clean. Prod.* **202**, 571–581 (2018).
39. Zhang, L., Li, Y., Guo, J., Kan, Z. & Jia, Y. Catalytic ozonation mechanisms of Norfloxacin using Cu–CuFe2O4. *Environ. Res.* **216**, 114521 (2023).
40. Tan, C. et al. Enhanced removal of coumarin by a novel O3/SPC system: kinetic and mechanism. *Chemosphere* **219**, 100–108 (2019).
41. Nabavi, S. R., Nazbakhsh, M. H., Rezvani, B., Jafarian, S. & Jourshabani, M. Catalytic ozonation of ciprofloxacin using MnO2/biochar nanohybrid integrated with peroxymonosulfate in a circulating fluidized bed reactor. *J. Water Process. Eng.* **69**, 106639 (2025).
42. Mojiri, A., Vakili, M., Farraji, H. & Aziz, S. Q. Combined ozone oxidation process and adsorption methods for the removal of acetaminophen and amoxicillin from aqueous solution; kinetic and optimisation. *Environ. Technol.*

Innov. **15**, 100404 (2019).

43. Zhang, D. et al. Synergistic effect of Fe and Ce on Fe doped CeO2 for catalytic ozonation of amoxicillin: Efficiency evaluation and mechanism study. *Sep. Purif. Technol.* **313**, 123430 (2023).
44. Dolatabadi, M. & Ahmadzadeh, S. Catalytic ozonation process using modified activated carbon as a cataly st for the removal of sarafloxacin antibiotic from aqueous solutions. *Anal. Methods Environ. Chem. J.* **6**, 31–41 (2023).
45. Martini, J., Orge, C. A., Faria, J. L., Pereira, M. F. R. & Soares, O. S. G. Catalytic advanced oxidation processes for sulfamethoxazole degradation. *Appl. Sci.* **9**, 2652 (2019).
46. Moussavi, G., Alahabadi, A. & Yaghmaeian, K. Investigating the potential of carbon activated with NH4Cl for catalyzing the degradation and mineralization of antibiotics in ozonation process. *Chem. Eng. Res. Des.* **97**, 91–99 (2015).
47. Zhang, H. et al. DBD plasma coupling MnO2-Fe3O4-cellulose acetate films for sulfamethoxazole degradation: Insight for catalytic ozonation and Fenton effect. *J. Water Process. Eng.* **53**, 103819 (2023).
48. Alzahrani, E. Chitosan membrane embedded with ZnO/CuO nanocomposites for the photodegradation of fast green dye under artificial and solar irradiation. *Analytical Chem. Insights* **13** (2018).
49. Fatoni, A. et al. Synthesis, characterization of polyvinyl alcohol-chitosan-ZnO/CuO nanoparticle film and its biological evaluation as an antibacterial agent against Staphylococcus aureus. *Al-Kimiya J. Ilmu Kim Terap*. **10**, 1–12 (2023).
50. Gindose, T. G. et al. Synthesis of PVA-assisted MnO2–CuO–ZnO–g-C3N4 quaternary nanocomposite for the degradation of methylene blue from industrial wastewater. *Heliyon* **10** (2024).
51. Vigneshwaran, S. et al. *A versatile nature of effective photocatalytic activity for degradation of the organic pollutant Rhodamine-B dye by PVA/ZnO/CuO nanocomposite* Vol. 35 (Nano-Structures & Nano-Objects, 2023).
52. Mubeen, K. et al. Band structure tuning of ZnO/CuO composites for enhanced photocatalytic activity. *Journal Saudi Chem. Society* **27** (2023).
53. Qomariyah, L. et al. Synergistic photocatalytic and adsorption capabilities of ZnO/chitosan/CMC for organic dye degradation under sunlight irradiation. *International J. Biol. Macromolecules* **305** (2025).

Figures

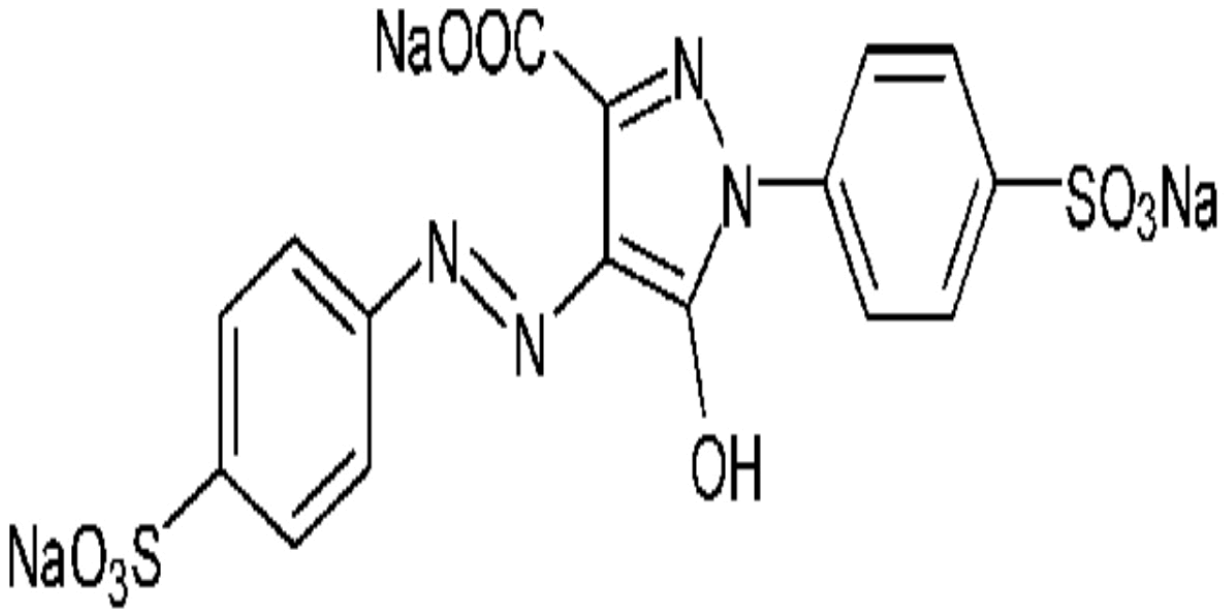


Figure 1

Chemical structure of Tartrazine

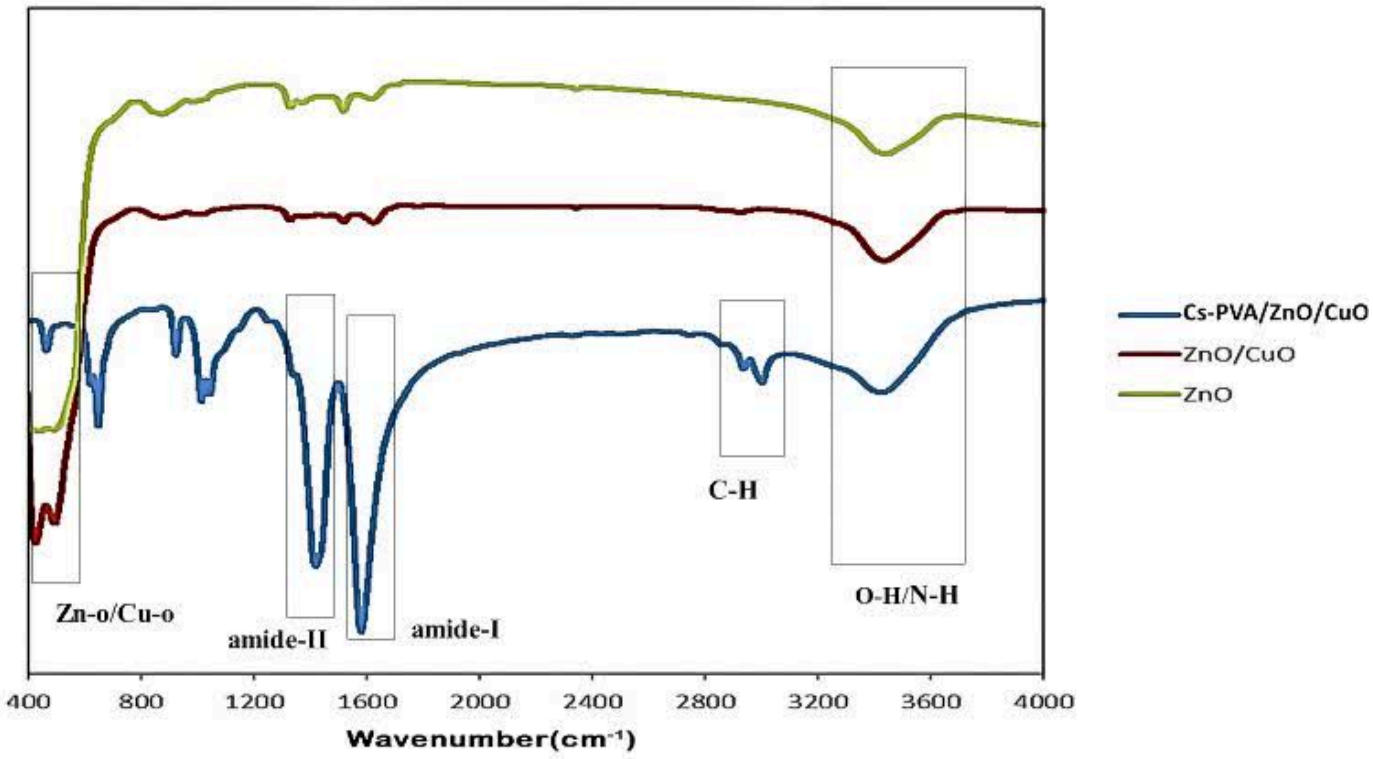


Figure 2

FTIR Spectra of CPZC nanocomposite

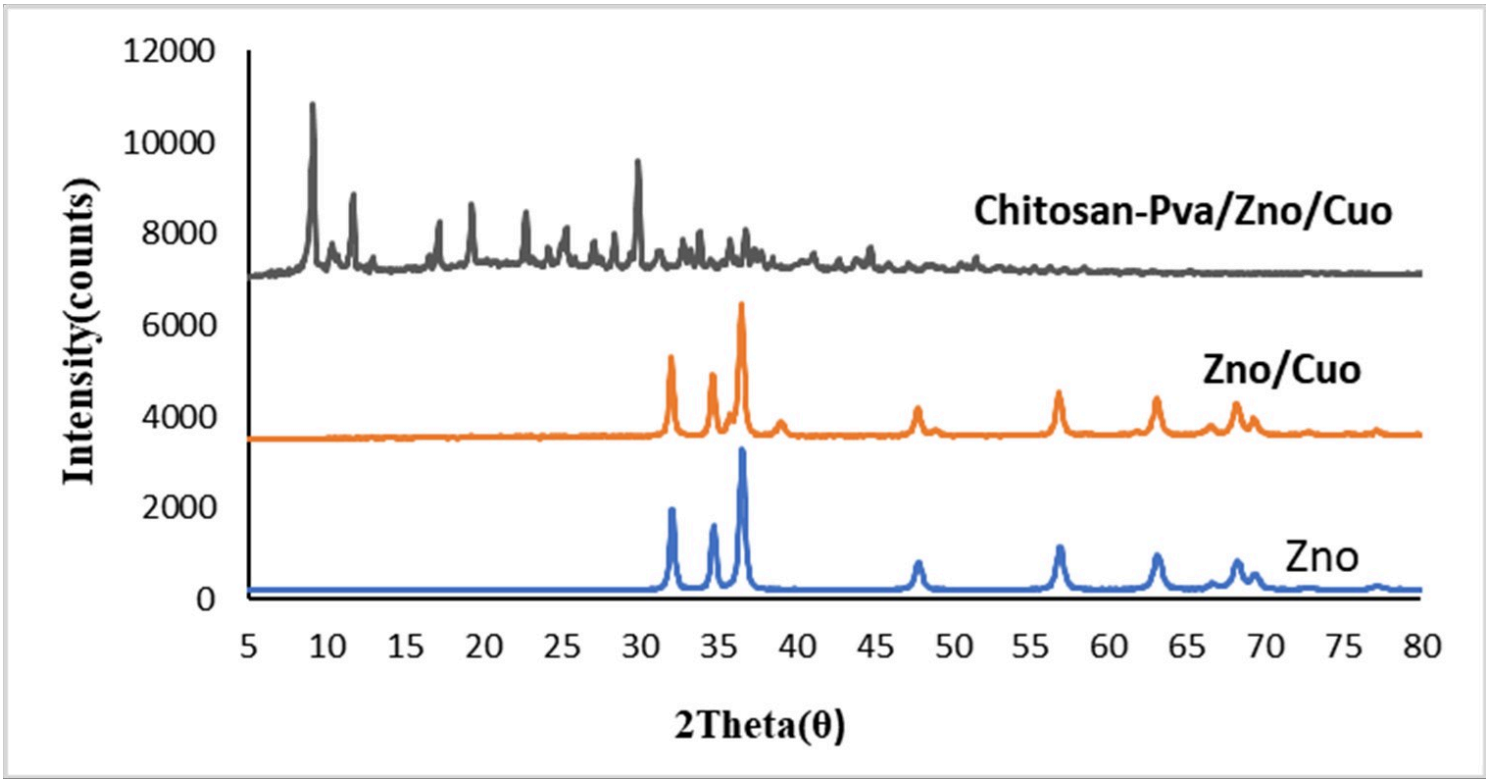


Figure 3

XRD spectra of CPZC nanocomposite.

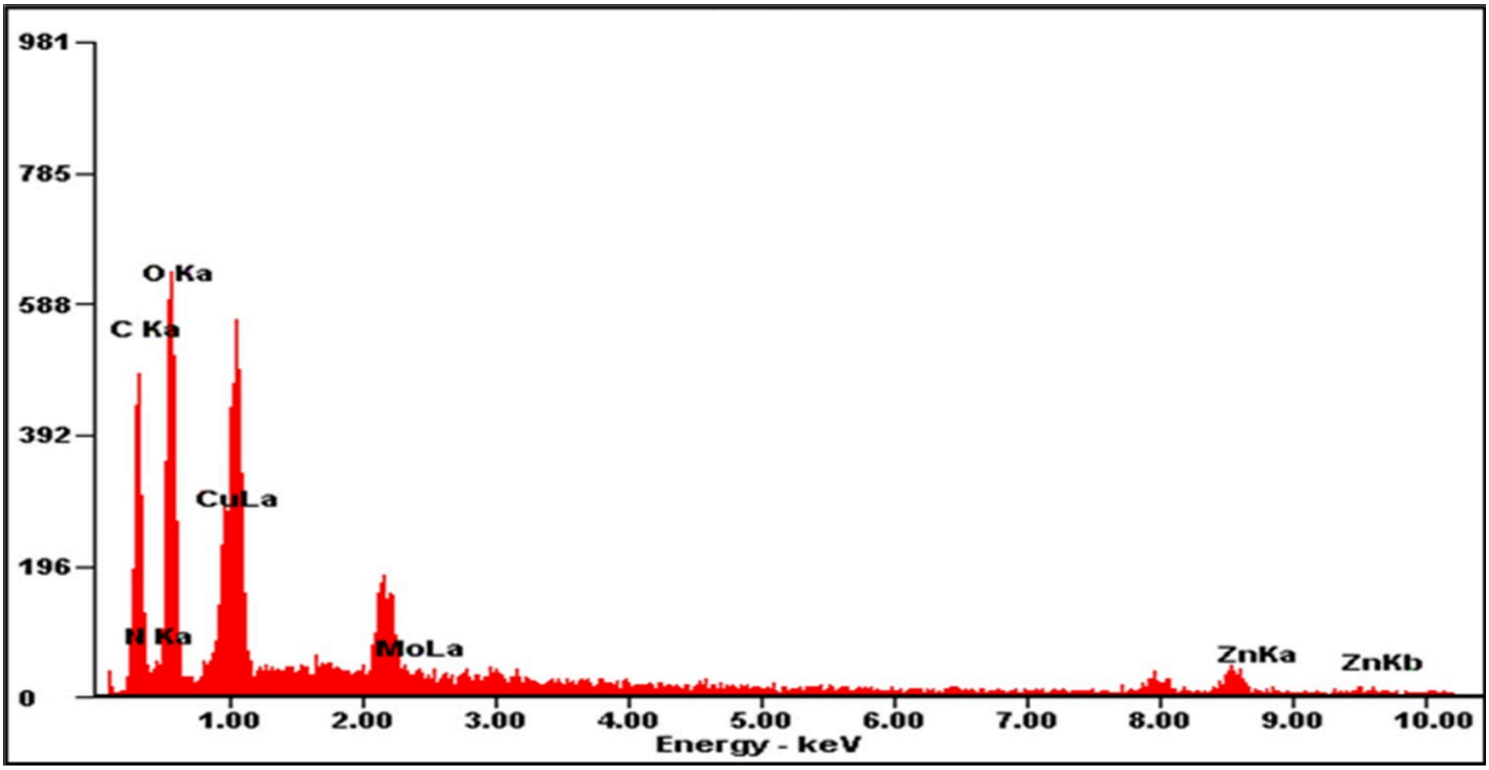


Figure 4

EDS spectra of CPZC nanocomposite

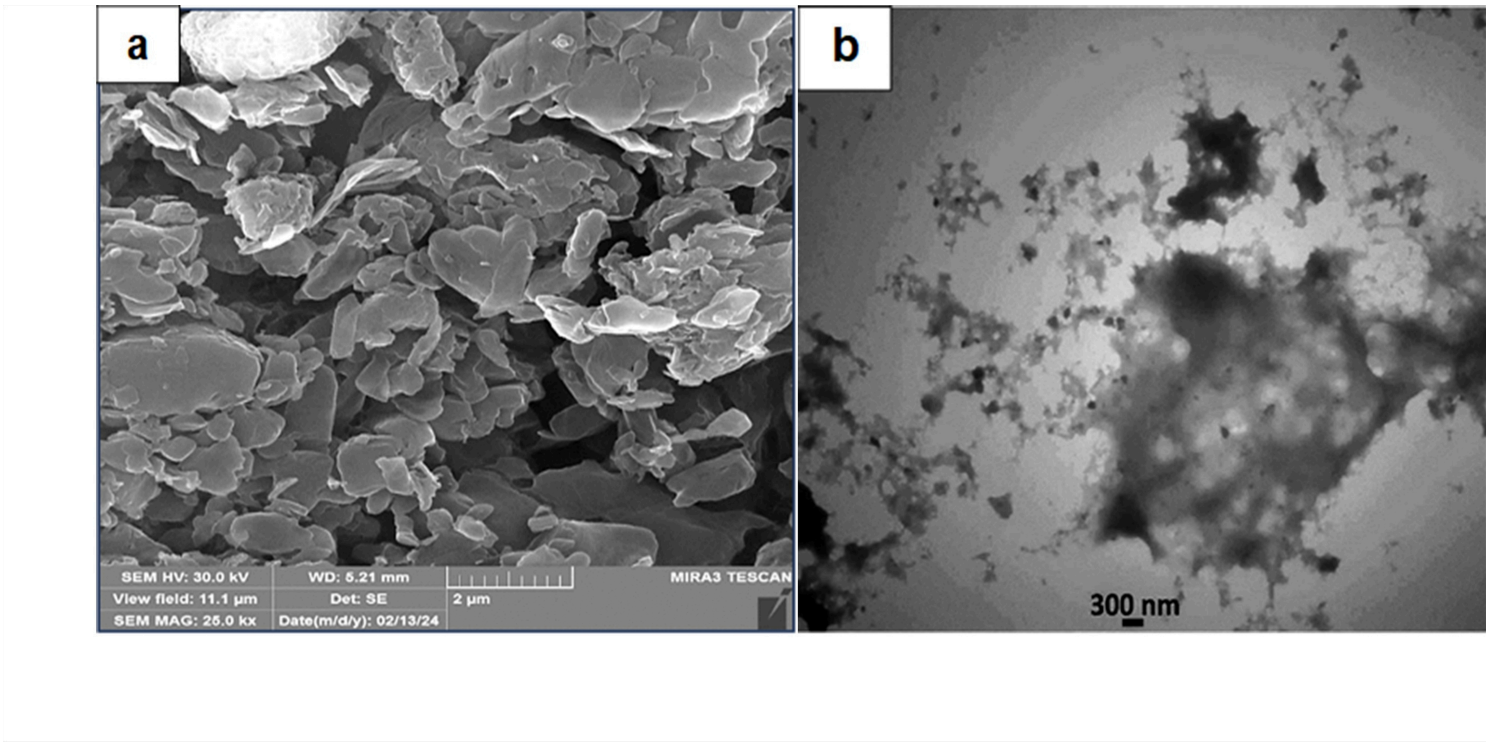


Figure 5

(a) FESEM spectra and (b) TEM spectra of CPZC nanocomposite

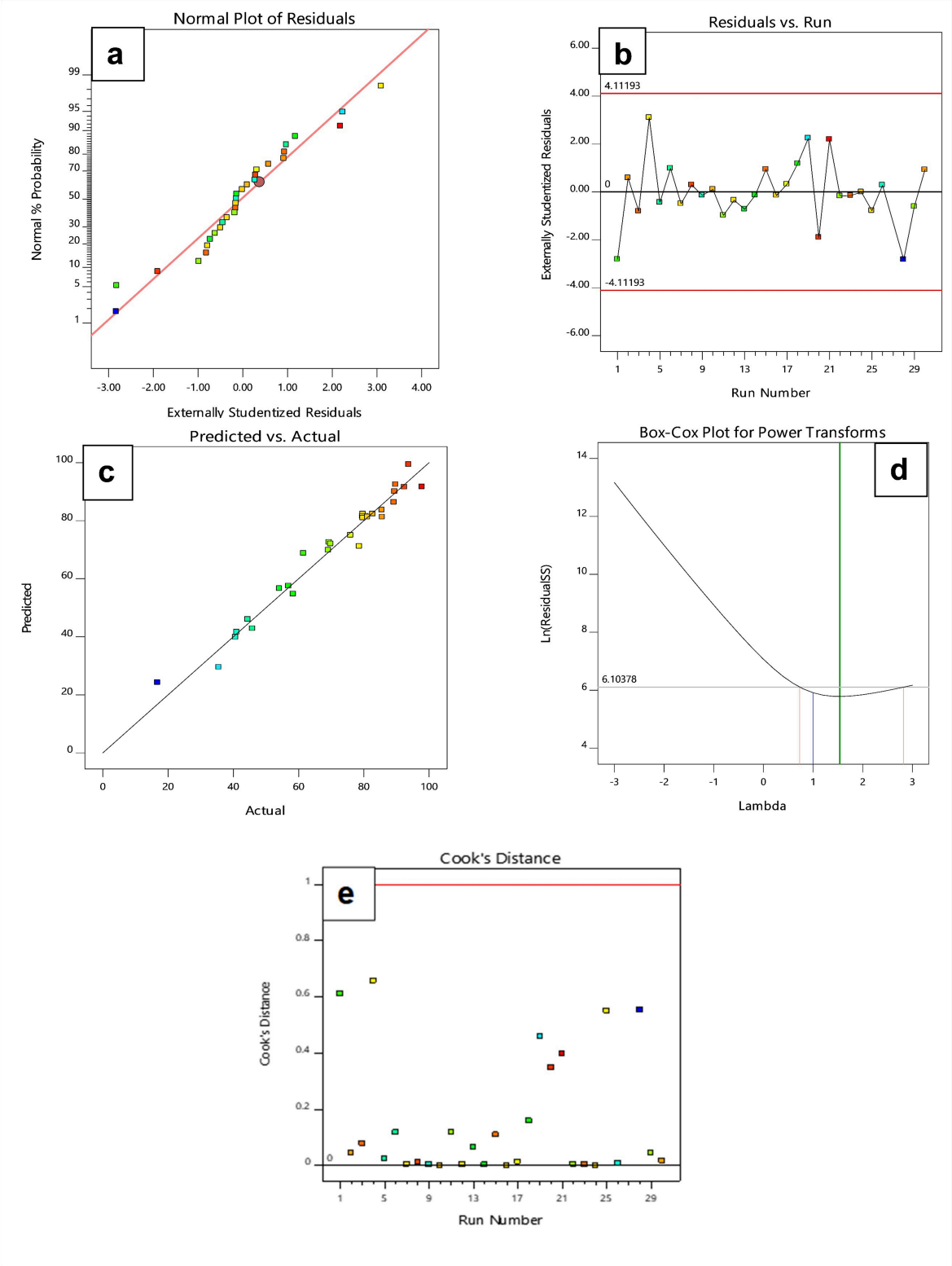


Figure 6

Normal Plot of Residual (a) Residual Vs. Run (b) Predicted Vs. Actual (c) Box -Cox Plot (d) Cook's Distance (e)

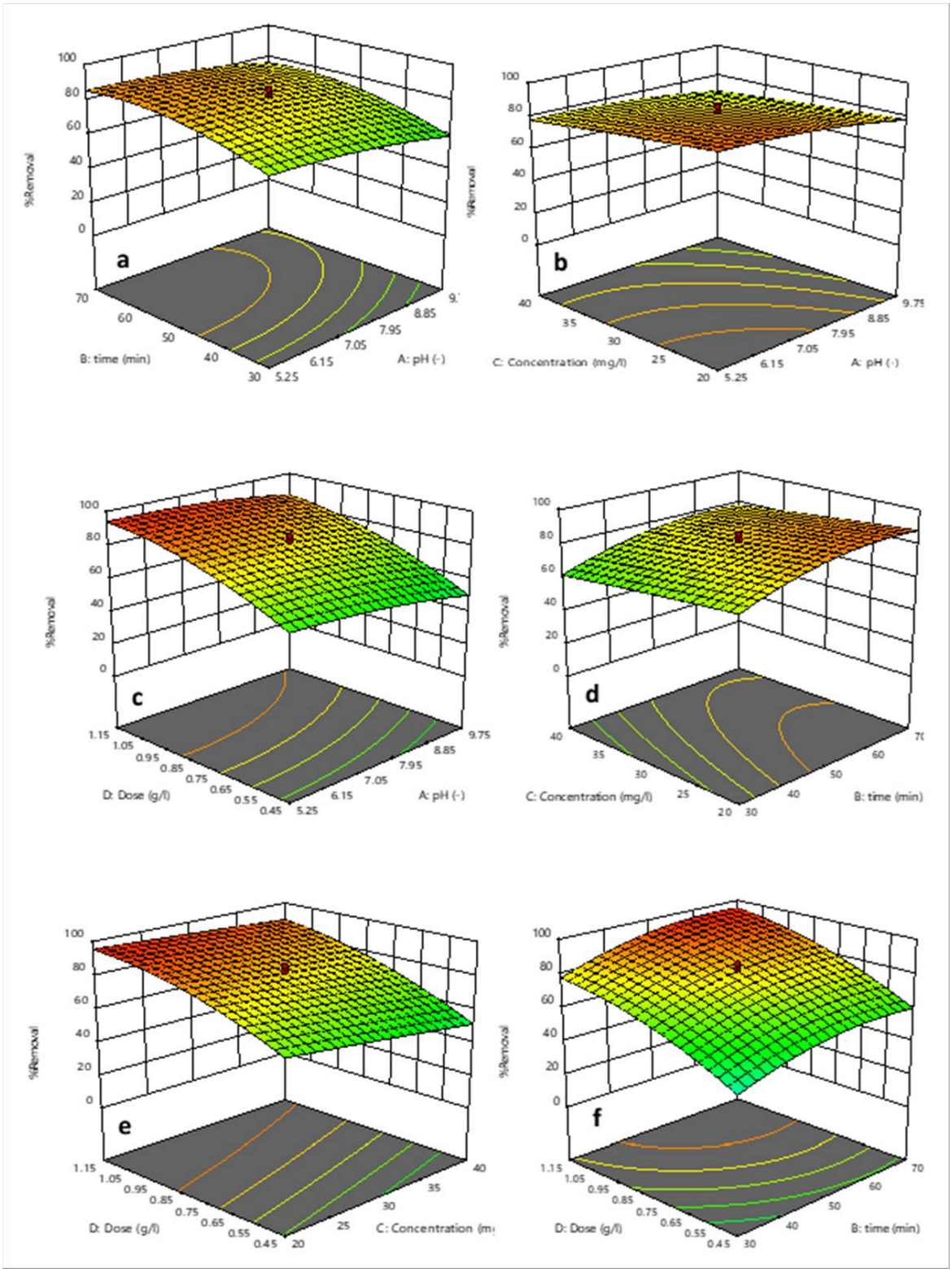


Figure 7

The wireframe plots of CPZC nanocomposite, (a) contact time and solution pH, (b) tartrazine initial concentration and solution pH, (c) the nanocomposite dosage and solution pH, (d) contact time and tartrazine initial concentration, (e) the nanocomposite dosage and tartrazine initial concentration (f) the nanocomposite dosage and contact time

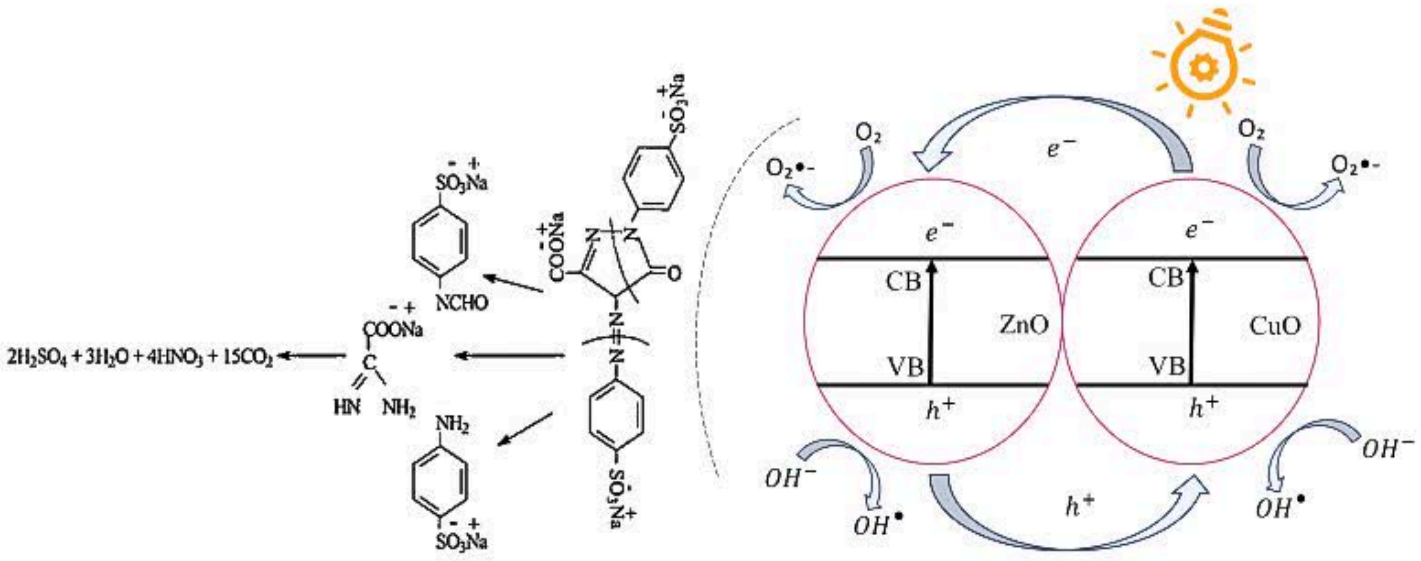


Figure 8

Conceptual scheme of the photocatalytic oxidation of tartrazine dye

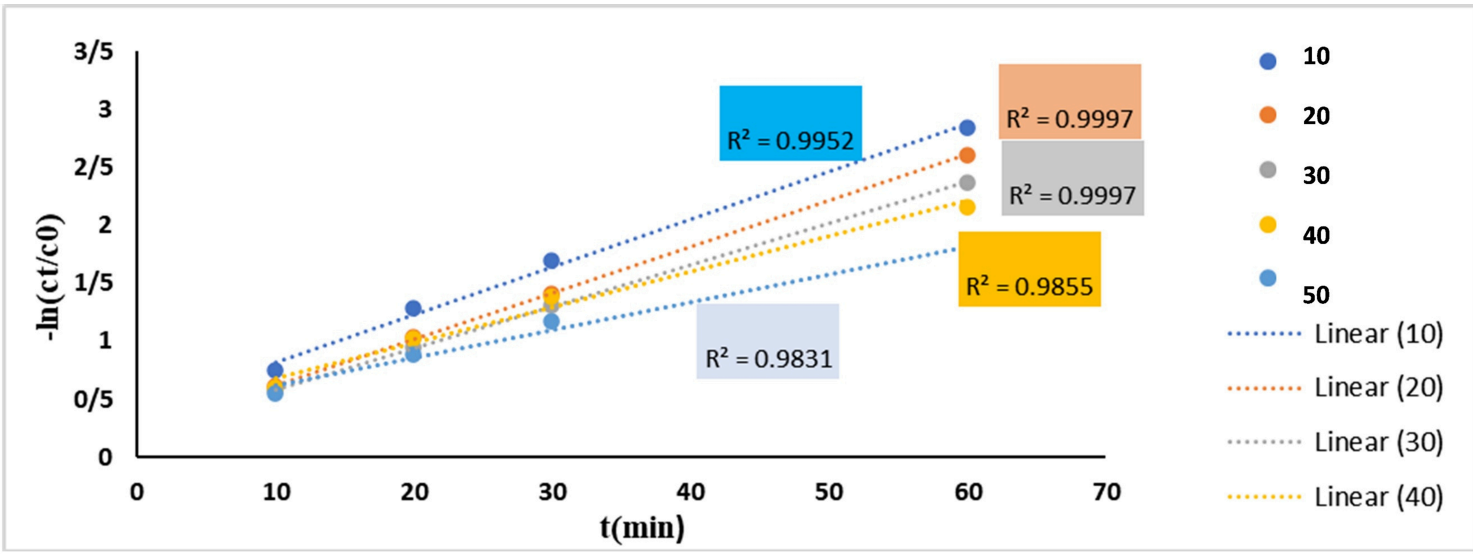


Figure 9

Kinetic Study of Tartrazine Dye Removal by Photocatalytic Oxidation Process Using CPZC nanocomposite